ChemPhysChem

Research Article
doi.org/10.1002/cphc.202400403

Chemistry Europe
European Chemical Societies Publishing

www.chemphyschem.org

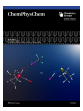

Similarities and Differences of Hydridic and Protonic Hydrogen Bonding

Maximilián Lamanec,[a, b, c] Jitka Zienertová,[a] Matej Špeťko,[b] Dana Nachtigallová,[a, b] and Pavel Hobza*[a, b]

Ab initio calculations were employed to investigate the interactions between selected electron-donating groups, characterized by M–H bonds (where M represents a transition metal and H denotes a hydridic hydrogen), and electron-accepting groups featuring both σ- and π-holes. The study utilized the ωB97X-D3BJ/def2-TZVPPD level of theory. Hydridic hydrogen complexes were found in all complexes with σ- and π-holes. A comparative analysis was conducted on the properties hydridic H-bond complexes, presented here and those studied previously, alongside an extended set of protonic H-bonds complexes. While the stabilization energies changes in M–H bond lengths, vibrational frequencies, intensities of the spectral bands, and charge transfer for these complexes are comparable, the nature of hydridic and protonic H-bonds fundamentally differ. In protonic H-bond complexes, the main stabilization forces arise from electrostatic contributions, while in hydridic H-bond complexes, dispersion energy, is the primary stabilization factor due to the excess of electrons and thus larger polarizability at hydridic H. The finding represents an important characteristic that distinguishes hydridic H-bonding from protonic H-bonds.

Introduction

The 2011 IUPAC definition of an X–H···Y hydrogen bond[1] (H-bond) specifies X as an atom possessing greater electronegativity than hydrogen, causing a partial positive charge on the hydrogen atom, commonly termed protonic hydrogen. In this context, Y serves as an electron donor. In the periodic table, only nine elements (C, N, O, F, Cl, Br, I, S, Se) exhibit higher electronegativity than hydrogen. The remaining elements are less electronegative (or more electropositive), leading to a partial negative charge on hydrogen, termed as hydridic hydrogen. In such cases, Y acts as an electron acceptor. Strictly following the IUPAC definition, such interactions cannot be classified as H-bonds. Rozas and Jablonski, in their computational studies on these complexes, referred to them as "inverse H-bond"[2] and "charge-inverted H-bond"[3–9] In our recent research,[10] we conducted low-temperature IR spectroscopy and computational methods to investigate complexes formed between trimethylsilane, which contains hydridic hydrogen, and various electron acceptors. These complexes demonstrate characteristics reminiscent of the classical (protonic) hydrogen-bonded complexes, such as the well-known red or blue shifts in the X–H stretching frequencies upon complex formation, along with an increase in the intensity of this spectral band. We proposed either maintaining the usage of the terms "protonic" and "hydride" H-bonding or rather the adopting a new definition of H-bonding that includes both types.[10]

This study explores other complexes featuring hydridic H-bonds formed between electron donors containing hydridic hydrogen covalently bound to transition metal d-orbitals (Fe, Mo, Ru, Rh, W, Re, Os, and Au), and electron acceptors with positive σ- and π-holes. The aim of the study is to explore the similarities and/or differences between both types of H-bonding not only in the set of complexes considered in the present paper but also in the previously studied complexes of both types.

Systems Investigated

Following molecules containing hydridic hydrogen covalently bound to more electropositive transition metal **Fe**$(Cp)(CO)_2H$, **Mo**$(Cp)(CO)_2)(PMe_3)H$, **Ru**$(Cp)(CO)_2H$, **Rh**$(CO)(PMe_3)_3H$, **W**$(Cp)(CO)_2$(*iMe*)H, **Re**(*bipy*)$(CO)_3H$, **Os**$(Cp)(CO)_2H$, **Au**(*iPr*)H with electron acceptor containing σ- and π-holes (ICF_3, BrCN; C_6F_6) were considered. Structures of all subsystems are provided in Figure S1, and their cartesian coordinates in Å are available in Supporting Information. The energy differences between the singlet, triplet, and quintet states (Table S1) confirm that the singlet state is the most stable for all hydrides.

The distinctive electronic and chemical properties of transition metal hydrides investigated make them indispensable

[a] M. Lamanec, J. Zienertová, D. Nachtigallová, P. Hobza
Institute of Organic Chemistry and Biochemistry of the Czech Academy of Sciences, Flemingovo náměstí 542/2, 160 00 Prague 6, Czech Republic
E-mail: pavel.hobza@uochb.cas.cz

[b] M. Lamanec, M. Špeťko, D. Nachtigallová, P. Hobza
IT4Innovations, VŠB-Technical University of Ostrava,
17. listopadu 2172/15, 708 00 Ostrava-Poruba, Czech Republic

[c] M. Lamanec
Department of Physical Chemistry, Palacký University Olomouc,
tr. 17. listopadu 12, 771 46 Olomouc, Czech Republic

Supporting information for this article is available on the WWW under https://doi.org/10.1002/cphc.202400403

in various fields of chemistry and engineering. They play a crucial role in catalytic hydrogenation,[11,12] where the breaking of H–H bonds generates metal hydride intermediates. These intermediates facilitate hydride transfer to unsaturated substrates, thus playing a crucial role in processes like C–H bond activation, including transfer hydrogenation,[11,13] olefin isomerization,[14,15] and C–H functionalization.[14–16] In energy conversion, transition metal hydrides participate in electrochemical reduction and catalyst protonation, initiating hydride transfer reactions with proton sources or carbon dioxide, ultimately yielding H_2 or carbon-based fuels.[17,18] Furthermore, these hydrides find applications in catalysts for reversible H_2 storage and serve as materials for bulk H_2 storage.[19,20]

Computations

Geometries of all subsystems and complexes were optimized at the ωB97X-D3BJ[21,22]/def2-TZVPPD[23] level. Harmonic vibration frequencies, evaluated under the rigid rotor-harmonic oscillator-ideal gas approximation, were determined at the same theoretical level. Natural Bond Orbital (NBO) charges and Wiberg Bond Indexes were obtained with NBO7[30] program. These calculations were performed with the ORCA 5.0.4[24] software. Electrostatic potentials were calculated using Molpro 2023[25,26] at the ωB97X-D3/def2-QZVPP level of theory. For energy decomposition analysis, the SAPT 2 + 3[27] method was employed, utilizing an aug-cc-pwCVTZ[28] basis set (aug-cc-pwCVTZ-PP for Mo and heavier elements, due to convergence failure, was replaced by def2-TZVPPD basis set for W atom), as implemented in the PSI4 1.9 program package.[29]

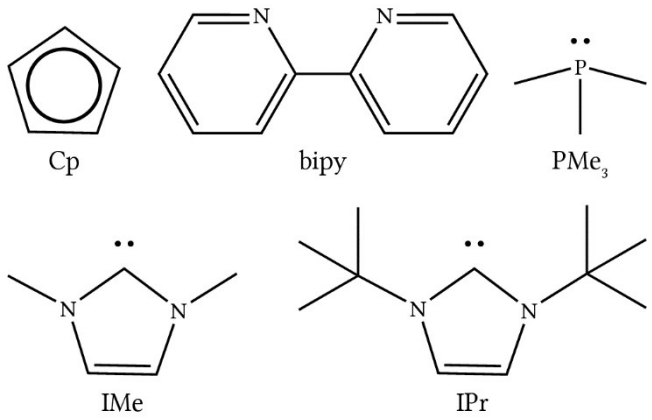

Scheme 1. Schemes and Abbreviations for Ligands.

Results and Discussion

Subsystems

Scheme 1 illustrates the fragments that compose the transition metal species with hydridic hydrogen, i.e, electron donors. Table 1 reports the key parameters of hydridic M–H bonds, such the M–H bond distance, Wiberg Bond Index (WBI), stretching frequency, atomic charge (q), and the minimal value of electrostatic potential ($V_{S,min}$) on hydridic H atom. Since atomic charges are sensitive to the size of the basis set used, we determined them also with larger def2-QZVPPD basis set. From the Table 1 it is evident that significant enlargement of basis set results in only negligible changes of hydridic atomic charges. The highest $V_{s,min}$ values were recorded in the Au(*iPr*)H and Re(*bipy*)$(CO)_3$H systems, with values of −39.2 and −38.1 kcal/mol, respectively. These results highlight the substantial hydride nature of the hydrogen atoms in these systems, where hydrogen forms covalent bonds with gold (Au) and rhenium (Re). On the contrary, in the Ru(Cp)$(CO)_2$H system, with a $V_{s,min}$ value of −8.9 kcal/mol, the hydrogen atom exhibits significantly less hydride nature. It is worth noting that $V_{s,min}$ of hydridic hydrogen in trimethylsilane studied in our group recently amounts to −8.8 kcal/mol. In the systems studied, hydridic hydrogen atoms are shielded by neighboring atoms or groups which provide steric hindrance for most electron donors. An exception is Re(*bipy*)$(CO)_3$H, where all atoms lie in a plane except for the –CO group and the -H atom, which are perpendicular to the plane formed by Re(*bipy*). This structural arrangement makes the hydride hydrogen more accessible for interaction. The electron acceptors selected for complexation included those with σ- (ICF_3 and BrCN) and π-hole (C_6F_6). Among them, BrCN exhibits the highest $V_{s,max}$ value of 43.3 kcal/mol,

Table 1. M–H bond distances in monomers (in Å), Wiberg Bond Indices (WBI) and the stretching frequency for the M–H bond, and the minimal values of Electrostatic Potential ($V_{s,min}$ in kcal/mol) and NBO atomic charge at the hydridic hydrogen atoms calculated at the ωB97X-D3BJ/def2-TZVPPD level (ωB97X-D3/def2-QZVPP for ESP).

	r(M–H)	WBI(M–H)	ν(M–H)	$V_{s,min}$ (hydridic H)	$q_{NBO}(H)^{[a]}$	$q_{NBO}(H)^{[b]}$
Fe(Cp)$(CO)_2$H	1.484	0.587	2037.5	−11.95	0.016	0.018
Mo(Cp)$(CO)_2(PMe_3)$H	1.698	0.599	1915.3	−18.92	0.072	0.069
Ru(Cp)$(CO)_2$H	1.585	0.635	2116.0	−8.86	0.009	0.008
Rh(CO)$(PMe_3)_3$H	1.614	0.456	1963.3	−14.39	−0.146	−0.156
W(Cp)$(CO)_2$(*IMe*)H	1.826	0.607	1933.2	−25.52	0.035	0.028
Re(*bipy*)$(CO)_3$H	1.754	0.514	1805.3	−38.13	−0.258	−0.255
Os(Cp)$(CO)_2$H	1.620	0.669	2191.6	−13.80	−0.027	−0.025
Au(*IPr*)H	1.621	0.692	2081.6	−39.23	−0.374	−0.376

[a] Calculated in def2-TZVPPD basis set; [b] Calculated in def2-QZVPPD basis set.

followed by ICF_3 and C_6F_6 with $V_{s,max}$ values of 32.2, and 18.1 kcal/mol, respectively.

Complexes with σ-Hole Acceptors, ICF_3 and BrCN

Figures 1 and 2 depict the complexes of M–H electron donors with ICF_3 *and* BrCN electron acceptors, respectively. Their interaction energies (Table 2) are large, with stabilization energies ranging from 4 to 12 kcal/mol, compared to those calculated for complexes with trimethylsilane (3.7 kcal/mol and 3.2 kcal/mol for $(CH_3)SiH$-ICF_3 and $(CH_3SiH$-BrCN complexes, respectively (cf. Table S2)) in agreement with the smaller $V_{s,min}$ of its hydridic hydrogen. Tables 2 and S2 collectively gather stabilization energies of 30 complexes with hydridic H-bonds, all falling within the interval of 2 to 12 kcal/mol. For comparison, the interaction energies calculated for 262 neutral complexes with different types of protonic H-bonding (X–H···O/N) using the DFT-SAPT technique[31,32] lie in the interval of 3 to 9 kcal/mol, i.e. they are comparable with hydridic H-bond complexes. It is important to note that strong H-bonds, as defined by Desiraju and Steiner,[33] with stabilization energies up to 40 kcal/mol involve ionic rather than neutral systems.

Comparison of total and intrinsic interaction energies of complexes presented in Table 2 reveals a small to negligible role of deformation energies. The properties of intermolecular

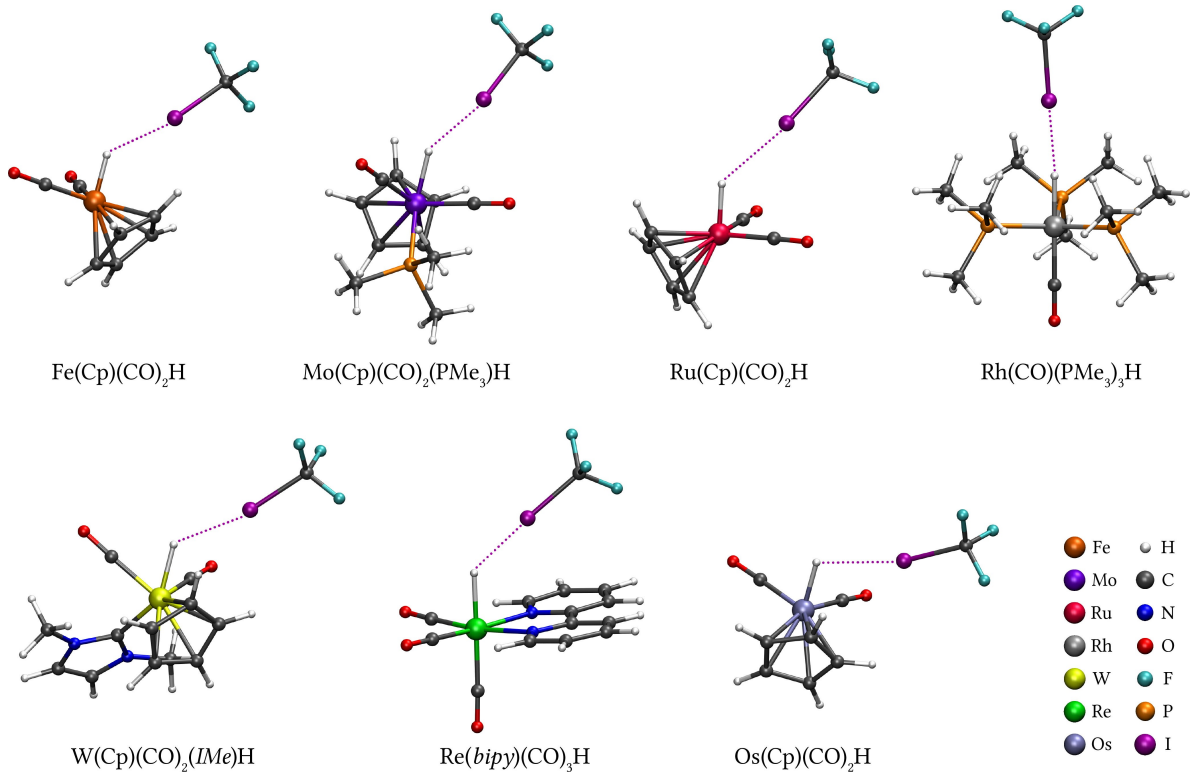

Figure 1. Structures of complexes with ICF_3 optimized at ωB97X-D3BJ/def2-TZVPPD level.

Table 2. Total interaction energies (ΔE^T, kcal/mol) and intrinsic interaction energies (ΔE^I, kcal/mol) calculated at the ωB97X-D3BJ/def2-TZVPPD level.

	ICF_3		BrCN		C_6F_6	
	ΔE^T	ΔE^I	ΔE^T	ΔE^I	ΔE^T	ΔE^I
$Fe(Cp)(CO)_2H$	−5.54	−5.72	−4.77	−4.92	–[b]	
$Mo(Cp)(CO)_2(PMe_3)H$	−6.58	−6.86	−5.96	−6.17	–[b]	
$Ru(Cp)(CO)_2H$	−4.20	−4.41	−3.91	−4.05	–[b]	
$Rh(CO)(PMe_3)_3H$	−9.24	−9.51	−7.36	−7.76	−8.66	−8.88
$W(Cp)(CO)_2$ (*IMe*)H	−7.47	−7.88	−6.94	−7.21	−7.58	−7.73
Re(*bipy*)$(CO)_3H$	−11.86	−12.62	−10.43	−10.82	–[b]	
$Os(Cp)(CO)_2H$	−6.23	−6.46	−5.24	−5.40	–[b]	
Au(*IPr*)H	–[a]		−10.10	−10.40	−9.32	−9.32

[a] No minima involving H···I interaction found for the complex; [b] No minima involving H···π interaction found for the complex.

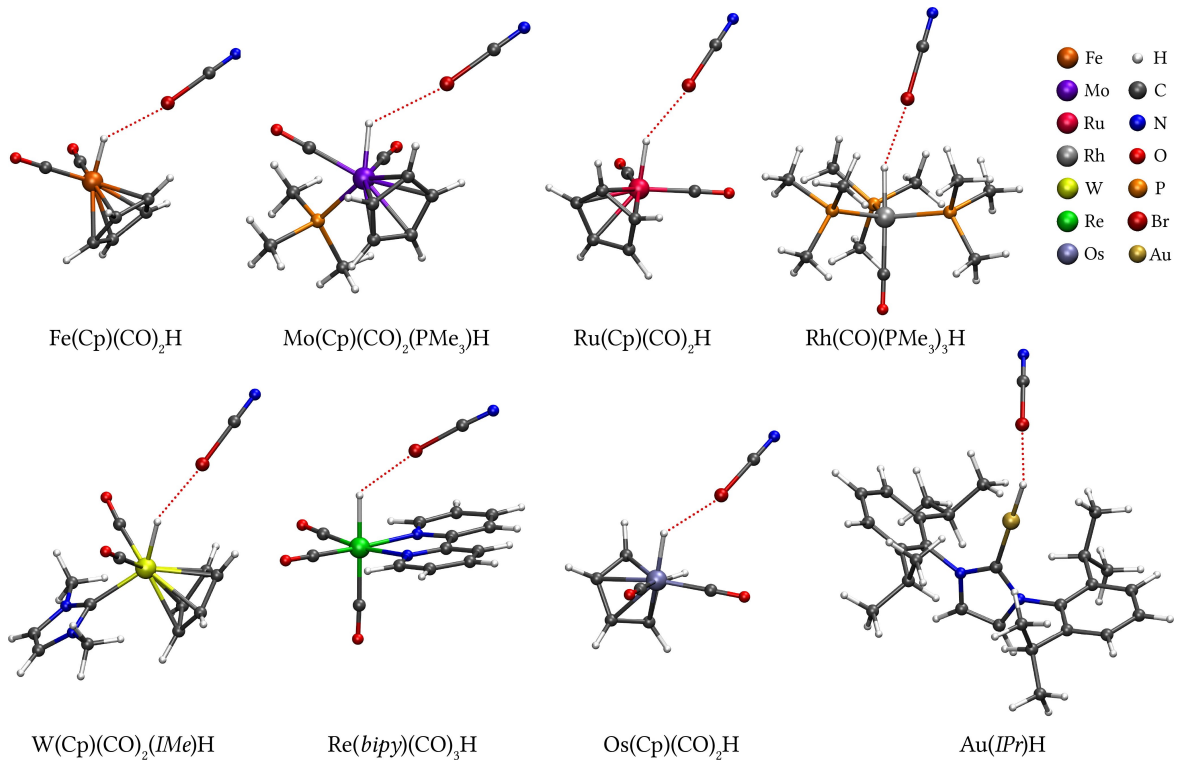

Figure 2. Structures of complexes with BrCN optimized at ωB97X-D3BJ/def2-TZVPPD level.

bonds H···Y (Y = Br, I, Table 3), such as distances in the range of 2.4 to 2.8 Å and small WBI values of less than 0.1, correspond to those observed in other hydridic or protonic H-bonds. Similarly, the changes observed in the M–H bond, such as changes in its length, shifts in vibration frequency, and increase in intensity, fulfill the criteria of the H-bond. Except Rh-containing complexes, the M–H bonds slightly elongate upon complex formation, resulting in a redshift in vibrational frequencies. Small shortenings of the Rh–H bond in $Rh(CO)(PMe_3)_3H$ complexes with ICF_3 and BrCN lead to the blue shifts of the M–H stretching frequency. In addition to the largest stabilization energies of Re-containing complexes, all indicators of H-bond strength, such as the elongation of the Re–H bond, the associated magnitude of the red shift and intensity of the vibrational frequency, as well as the value of WBI and the reduction of the WBI of the Re–H bond by complexation, point to the strongest H-bond among the transition metals studied. These findings can be explained not only by its highest $V_{s,min}$ but also by a planar structure of the Re(*bipy*) core, which enhances the accessibility of hydridic hydrogen, as discussed earlier. The results presented in Table 4 demonstrate the character of H-bonds in terms of charge transfer, obtained from the comparison of charges on transition metals and hydrogen atoms of M–H bonds calculated for monomers and corresponding complexes, as well as the value of charge calculated for M–H fragment in M–H···Y complex, denoted as q(hydride). Although the calculated changes of q(H) and q(M) are small, there is a general tendency for an increase in the electron density of q(H) upon complexation. These changes range from 0.02–0.07 e^-, with the largest values observed for $Rh(CO)(PMe_3)_3H$. The values of q(hydride) indicate that electron density is transferred from electron-donating M–H to electron-accepting Y fragments, with changes ranging from 0.01 to 0.06 e^-. The small changes in charge distribution on one side and the unambiguous identification of H-bonding using IR spectral characteristics are somewhat surprising. Unfortunately, the NBO analysis which could provide explanation in terms of electron transfer among different orbitals of the complex, cannot be applied due to the failure to correctly separate the complexes to their fragments. Nevertheless, we were able to explain this phenomenon in our previous study on hydridic H-bonds in complexes of trimethylsilane[10] where the NBO analyses pointed out not only to donation from electron donor to electron acceptor but also to back-donation in the reversed direction.

Complexes with π-Hole Acceptor C_6F_6

The structure minimizations led to only three stable complexes with C_6F_6 displayed in Figure 3. The resulting interaction energies are reported in Table 2. The failure to obtain other stable complexes is most likely the result of (i) steric constraints that prevent C_6F_6 from accessing the π-hole for an effective interaction and (ii) weaker electron-accepting property, as shown by calculated value of $V_{s,max}$, discussed earlier. However, the stabilization energies of $Rh(CO)(PMe_3)_3H$, $W(Cp)(CO)_2$(*IMe*)H, and Au(*IPr*)H complexes are high (up to 9 kcal/mol) and are

Table 3. Intramolecular (M–H) and intermolecular (H···X) bond distances (in Å), along with their respective Wiberg bond indexes (WBI). Spectral characteristics for M–H stretching frequency are also included, denoting both the shift (ν in cm^{-1}) and intensity (ΔI in km/mol).

A	ICF_3					
	Δr(M–H)	WBI(M–H)	r(H···I)	WBI(H···I)	Δν(M–H)	ΔI(M–H)
$Fe(Cp)(CO)_2H$	0.006	0.576	2.770	0.022	−24.6	150.1
$Mo(Cp)(CO)_2(PMe_3)H$	0.006	0.589	2.703	0.025	−16.8	119.7
$Ru(Cp)(CO)_2H$	0.004	0.615	2.757	0.022	−16.3	112.6
$Rh(CO)(PMe_3)_3H$	−0.003	0.411	2.630	0.065	46.9/23.4	0.1/805.2
W(Cp)$(CO)_2$(*IMe*)H	0.006	0.596	2.401	0.028	−13.1	456.4
Re(*bipy*)$(CO)_3H$	0.016	0.449	2.405	0.081	−34.8	668.9
$Os(Cp)(CO)_2H$	0.004	0.650	2.832	0.018	−12.7	57.6
B	BrCN					
	Δr(M–H)	WBI(M–H)	r(H···Br)	WBI(H···Br)	Δν(M–H)	ΔI(M–H)
$Fe(Cp)(CO)_2H$	0.005	0.581	2.708	0.014	−15.5	100.4
$Mo(Cp)(CO)_2(PMe_3)H$	0.005	0.598	2.708	0.013	−13.3	59.8
$Ru(Cp)(CO)_2H$	0.004	0.621	2.724	0.013	−12.1	59.5
$Rh(CO)(PMe_3)_3H$	−0.002	0.431	2.425	0.036	37.0/17.5	−9.9/382.7
W(Cp)$(CO)_2$(*IMe*)H	0.005	0.604	2.632	0.016	−8.6	80.0
Re(*bipy*)$(CO)_3H$	0.013	0.473	2.442	0.042	−35.4	358.6
$Os(Cp)(CO)_2H$	0.004	0.656	2.793	0.011	−10.4	51.7
Au(*IPr*)H	0.056	0.642	2.703	0.030	−30.7	−19.77
C	C_6F_6					
	Δr(M–H)	WBI(M–H)	r(H···π-hole)[a]	Δν(M–H)	ΔI(M–H)	
$Rh(CO)(PMe_3)_3H$	0.003	0.452	2.837	0.8/2.1	−12.8/74.6	
W(Cp)$(CO)_2$(*IMe*)(H	−0.012	0.595	2.491	14.9	1339.9	
Au(*IPr*)H	0.058	0.671	2.726	22.7	−30.9	

[a] Distance is defined between the hydrogen atom of the hydride and the geometric center of the C_6F_6 molecule.

Table 4. Difference in charges on hydrogen atom (from M–H bond), on M and total charge of hydride molecule in monomers and complexes with ICF_3 and BrCN.

	Monomers		ICF_3			BrCN		
	q(H)	q(M)	q(H)	q(M)	q(hydride)	q(H)	q(M)	q(hydride)
$Fe(Cp)(CO)_2H$	0.016	−0.339	−0.026	−0.339	0.015	−0.026	−0.332	0.011
$Mo(Cp)(CO)_2(PMe_3)H$	0.072	−0.633	0.023	−0.640	0.014	0.028	−0.640	0.009
$Ru(Cp)(CO)_2H$	0.009	−0.229	−0.036	−0.220	0.010	−0.034	−0.220	0.007
$Rh(CO)(PMe_3)_3H$	−0.145	−0.385	−0.213	−0.367	0.031	−0.205	−0.371	0.020
W(Cp)$(CO)_2$ (*IMe*)H	0.034	−0.198	−0.019	−0.196	0.020	−0.013	−0.199	0.013
Re(*bipy*)$(CO)_3H$	−0.258	−0.242	−0.297	−0.240	0.064	−0.302	−0.243	0.034
$Os(Cp)(CO)_2H$	−0.027	−0.001	−0.049	−0.014	0.023	−0.027	−0.001	0.015

similar to these of stacked complexes of benzene with hexa-halogen-benzenes,[34] as well as with complexes featuring σ-hole acceptors reported in Table 2. The H···Y (Y = π-hole) intermolecular distances are in the same range, i.e., ranging from 2.5–2.8 Å. The changes in M–H bond distances (see Table 3) exhibit both elongation (for $Rh(CO)(PMe_3)_3H$ and Au(*IPr*)H) and contraction (for W(Cp)$(CO)_2$(*IMe*)H), accompanied systematically by blue-shifted stretching frequencies.

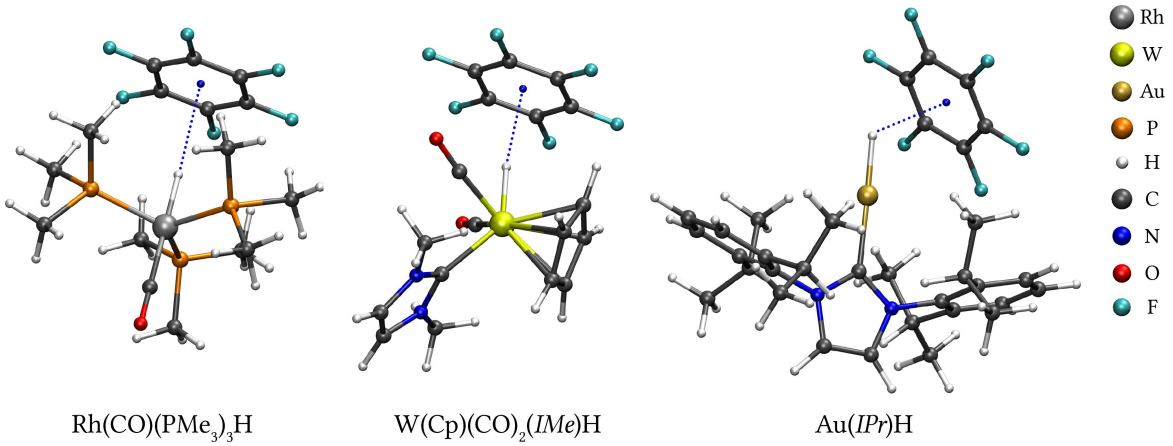

Figure 3. Structures of complexes with C_6F_6 optimized at ωB97X-D3BJ/def2-TZVPPD level.

Similarities and/or Differences of Hydridic and Protonic H-Bonds

In the preceding paragraphs as well as in our previous paper[10] where we investigated hydridic H-bonds both computationally and experimentally, we highlighted profound similarities between both types of H-bonds. More specifically, we observed similarities in the magnitude of stabilization energy, the elongation or contraction of the X–H bond upon complex formation accompanied by the red or blue shifts of the corresponding stretching frequency and increase in intensity of the respective spectral band. However, one distinctive feature sets apart both types of H-bonds, namely the dominance of a particular energy term. The IUPAC Recommendations 2011 in chapter 2.3 Footnotes, part F2 states that "Attractive interactions arise from electrostatic forces between permanent multipoles, inductive forces between permanent and induced multipoles and London dispersion forces. If an interaction is primarily due to dispersion forces, then it would not be characterized as a hydrogen bond ". There are different techniques used for energy partitioning. Among them the SAPT[35] which provides first- and second-order energy terms (including electrostatic and exchange-repulsion; induction and dispersion) is the most frequently used. Table 5 presents total SAPT interaction energy

Table 5. Intrinsic interaction energy and its components calculated using SAPT2+3 method. All energies in kcal/mol.

ICF_3					
	ΔE_{Elstat}	ΔE_{Exch}	ΔE_{Ind}	ΔE_{Disp}	$\Delta E^{SAPT2+3}$
$Fe(Cp)(CO)_2H$	−7.41	13.16	−3.60	−9.81	−7.65
$Mo(Cp)(CO)_2(PMe_3)H$	−7.57	14.41	−4.16	−11.25	−8.57
$Ru(Cp)(CO)_2H$	−4.40	10.02	−2.95	−8.17	−5.49
$Rh(CO)(PMe_3)_3H$	−11.95	23.88	−7.89	−15.46	−11.41
$W(Cp)(CO)_2$ (*IMe*)H	−9.26	16.91	−5.11	−12.22	−9.68
Re(*bipy*)$(CO)_3H$	−19.24	31.49	−10.36	−19.38	−17.49
$Os(Cp)(CO)_2H$	−8.10	15.14	−3.52	−11.46	−7.93
BrCN					
	ΔE_{Elstat}	ΔE_{Exch}	ΔE_{Ind}	ΔE_{Disp}	$\Delta E^{SAPT2+3}$
$Fe(Cp)(CO)_2H$	−5.36	9.20	−3.07	−7.17	−6.39
$Mo(Cp)(CO)_2(PMe_3)H$	−5.90	9.89	−2.90	−8.24	−7.15
$Ru(Cp)(CO)_2H$	−4.06	6.76	−1.45	−5.94	−4.68
$Rh(CO)(PMe_3)_3H$	−8.84	15.70	−4.96	−10.73	−8.83
$W(Cp)(CO)_2$ (*IMe*)H	−7.31	11.30	−3.50	−8.75	−8.26
Re(*bipy*)$(CO)_3H$	−14.43	20.57	−6.10	−13.90	−13.86
$Os(Cp)(CO)_2H$	−5.33	9.73	−2.82	−7.86	−6.27

as well as individual energy terms for 14 complexes featuring transition metals containing hydridic H-bonds. In 13 out of 14 complexes, the dispersion energy emerges as the dominant term, with the difference between leading electrostatic and dispersion energies in the remaining complex being less than 5%. Additionally, Table S3 presents these energies for 13 complexes of trimethylsilane with various electron acceptors, as examined in our previous paper also showing the dominance of the dispersion energy. Clearly, the significant role of dispersion energy cannot be attributed to the presence of highly polarizable transition metals but rather to the hydridic hydrogen, which possesses an excess of electron density (see later).

The situation with protonic H-bonding is fundamentally different. This conclusion stems from analysis of an extended set of 262 neutral complexes[31,32] with various types of H-bonding (X–H···O/N), where electrostatic energy was dominant in over 90% of cases.

To exclude the effect of the larger size of the hydridic complexes considered in Table 3, we added 14 small hydrogen-bonded complexes containing HBr and HI as hydrogen donors and various proton acceptors with heavier atoms. As shown in Table S4, in 13 out of the 14 complexes, the contribution of electrostatic interaction is larger or significantly larger than the dispersion contribution. In the one case of the HI···C_4H_8Te complex, the dispersion contribution is larger by 0.5 kcal/mol than the electrostatic contribution.

As mentioned previously, the significance of dispersion energy in complexes with hydridic H-bond is attributed to the excess of negative charge at hydridic hydrogen, leading to its large polarizability. This concept is exemplified by Re(*bipy*)$(CO)_3$H···BrCN and MeOH···NH_2Me complexes, which feature hydridic and protonic H-bonds. In the former complex, there is an excess electron (1.3 e), while in the latter there is a lack of electrons (0.5 e) at hydrogen atoms. The corresponding polarizabilities can be estimated using the calculated MP2 polarizabilities of the hydrogen atom with different electron densities: H^+, $H^\bullet$ and H^- (0, 1.4, and 3.6 Å^3 respectively). Extrapolation of these values to the current electron densities yields a ratio between dispersion energies for complexes with hydridic and protonic hydrogens of approximately 2–3 to 1. However, the situation with hydridic H-bonded complexes formed by hydrides of alkali metals or alkali earth metals may be different, as the electrostatic term will be more pronounced than in the before mentioned complexes.

Conclusions

Computational studies, employing the ωB97X-D3BJ/def2-TZVPPD level of theory, were conducted to characterize complexes formed between electron-donating groups exhibiting M–H pattern (where M represents transition metals such as Fe, Mo, Ru, Rh, W, Re, Os, and Au, and H denotes a hydridic hydrogen) and electron acceptors featuring σ- (ICF_3, BrCN) and π-hole (C_6F_6) characteristics. Hydridic H-bonds predominantly formed between electron donors with σ- and π-hole electron acceptors. These complexes exhibit stabilization energies similar to those of complexes with classical protonic H-bonds. In addition, both red- and blue-shifted hydridic H-bonds exhibited changes in metal-hydrogen (M–H) bond lengths upon complex formation, reflecting characteristics observed in protonic hydrogen-bonded complexes. These changes include variations in bond lengths, vibrational frequencies, and intensities of the respective spectral band. However, in contrast to complexes with protonic H-bonds, which are predominantly stabilized by electrostatic interactions, the complexes with hydridic H-bonds were found to be stabilized predominantly by dispersion terms. Analyses of electron density distributions revealed that the primary contributions from dispersion energy originate from the excess of electrons at the hydridic hydrogen. ***This finding represents a pivotal characteristic that sets apart hydridic H-bonding from protonic H-bonding.***

Acknowledgements

This article has been produced with the financial support of Palacký University through the Internal Grant Association, project IGA_PrF_2024_017 (M.L.), the Ministry of Education, Youth and Sports of the Czech Republic through the e-INFRA CZ (ID: 90254) (M.Š.), the European Union under the REFRESH – Research Excellence for Region Sustainability and High-tech Industries project number CZ.10.03.01/00/22_003/0000048 via the Operational Programme Just Transition (D.N. and P.H.). Open Access publishing facilitated by Ustav organicke chemie a biochemie Akademie ved Ceske republiky, as part of the Wiley - CzechELib agreement.

Conflict of Interests

The authors declare no conflict of interest.

Data Availability Statement

The data that support the findings of this study are available in the supplementary material of this article.

Keywords: hydrogen bond · charge inverted hydrogen bond · DFT · SAPT

[1] E. Arunan, et al., *Pure Appl. Chem.* **2011**, *83*, 1619–1636.
[2] I. Rozas, I. Alkorta, J. Elguero, *J. Phys. Chem. A* **1997**, *101*, 4236–4244.
[3] M. Jabłoński, *Chem. Phys. Lett.* **2009**, *477*, 374–376.
[4] M. Jabłoński, *J. Mol. Struct.* **2010**, *948*, 21–24.
[5] M. Jabłoński, *Chem. Phys.* **2014**, *433*, 76–84.
[6] M. Jabłoński, *J. Comput. Chem.* **2014**, *35*, 1739–1747.
[7] M. Jabłoński, *Chem. Phys. Lett.* **2009**, *477*, 374–376.
[8] M. Jabłoński, *Struct. Chem.* **2020**, *31*, 61–80.
[9] M. Jabłoński, *Comput. Theor. Chem.* **2012**, *998*, 39–45.
[10] S. Civiš, M. Lamanec, V. Špirko, J. Kubišta, M. Špet'ko, P. Hobza, *J. Am. Chem. Soc.* **2023**, *145*, 8559.
[11] S. E. Clapham, A. Hadzovic, R. H. Morris, *Coord. Chem. Rev.* **2004**, *248*, 2201–2237.

[12] A. Robertson, T. Matsumoto, S. Ogo, *Dalton Trans.* **2011**, *40*, 10304–10310.
[13] P. A. Dub, T. Ikariya, *ACS Catal.* **2012**, *2*, 1718–1741.
[14] M. Hassam, A. Taher, G. E. Arnott, I. R. Green, W. A. L. Van Otterlo, *Chem. Rev.* **2015**, *115*, 5462–5569.
[15] G. Hilt, *ChemCatChem* **2014**, *6*, 2484–2485.
[16] T. W. Lyons, M. S. Sanford, *Chem. Rev.* **2010**, *110*, 1147–1169.
[17] M. R. Dubois, D. L. Dubois, *Acc. Chem. Res.* **2009**, *42*, 1974–1982.
[18] V. S. Thoi, Y. Sun, J. R. Long, C. J. Chang, *Chem. Soc. Rev.* **2013**, *42*, 2388–2400.
[19] S. I. Orimo, Y. Nakamori, J. R. Eliseo, A. Züttel, C. M. Jensen, *Chem. Rev.* **2007**, *107*, 4111–4132.
[20] J. Graetz, *Chem. Soc. Rev.* **2008**, *38*, 73–82.
[21] J. Da Chai, M. Head-Gordon, *J. Chem. Phys.* **2008**, *128*, 8.
[22] Y. S. Lin, G. De Li, S. P. Mao, J. Da Chai, *J. Chem. Theory Comput.* **2013**, *9*, 263–272.
[23] F. Weigend, R. Ahlrichs, *Phys. Chem. Chem. Phys.* **2005**, *7*, 3297–3305.
[24] F. Neese, F. Wennmohs, U. Becker, C. Riplinger, *J. Chem. Phys.* **2020**, *152*, 22.
[25] H. J. Werner, P. J. Knowles, G. Knizia, F. R. Manby, M. Schütz, *Wiley Interdiscip. Rev.: Comput. Mol. Sci.* **2012**, *2*, 242–253.
[26] H. J. Werner, P. J. Knowles, F. R. Manby, J. A. Black, K. Doll, A. Heßelmann, D. Kats, A. Köhn, T. Korona, D. A. Kreplin, Q. Ma, T. F. Miller, A. Mitrushchenkov, K. A. Peterson, I. Polyak, G. Rauhut, M. Sibaev, *J. Chem. Phys.* **2020**, *152*, 144107.
[27] E. G. Hohenstein, C. D. Sherrill, *J. Chem. Phys.* **2010**, *133*, 1.
[28] K. A. Peterson, T. H. Dunning, *J. Chem. Phys.* **2002**, *117*, 10548.
[29] D. G. A. Smith, L. A. Burns, A. C. Simmonett, R. M. Parrish, M. C. Schieber, R. Galvelis, P. Kraus, H. Kruse, R. Di Remigio, A. Alenaizan, A. M. James, S. Lehtola, J. P. Misiewicz, M. Scheurer, R. A. Shaw, J. B. Schriber, Y. Xie, Z. L. Glick, D. A. Sirianni, J. S. O'Brien, J. M. Waldrop, A. Kumar, E. G. Hohenstein, B. P. Pritchard, B. R. Brooks, H. F. Schaefer, A. Y. Sokolov, K. Patkowski, A. E. Deprince, U. Bozkaya, R. A. King, F. A. Evangelista, J. M. Turney, T. D. Crawford, C. D. Sherrill, *J. Chem. Phys.* **2020**, *152*, 18.
[30] E. D. Glendening, C. R. Landis, F. Weinhold, *J. Comput. Chem.* **2019**, *40*, 2234–2241.
[31] J. Řezáč, *J. Chem. Theory Comput.* **2020**, *16*, 2355–2368.
[32] E. Masumian, A. D. Boese, *J. Chem. Theory Comput.* **2024**, *20*, 30–48.
[33] G. Desiraju, T. Steiner, *The Weak Hydrogen Bond*, Oxford, **2001**.
[34] K. Pluháčková, P. Jurečka, P. Hobza, *Phys. Chem. Chem. Phys.* **2007**, *9*, 755–760.
[35] B. Jeziorski, R. Moszynski, K. Szalewicz, *Chem. Rev.* **1994**, *94*, 1887–1930.

Manuscript received: April 9, 2024
Revised manuscript received: May 21, 2024
Accepted manuscript online: May 21, 2024
Version of record online: July 10, 2024